Electronic Supplementary Material (ESI) for Materials Chemistry Frontiers.

Supplementary information

Design and synthesis of S-Scheme TiO_2 homojunction with adjusted well-defined phase for a directional carrier transfer in solar water splitting

Xiaobing Wang[a,*], Yihao Zhang[a,‡], Yu Cao[a,‡], Zhi Zheng[b,*], Xiaowei Guo[a,c], Jiabao Cui[a], Xiangdong Lou[a], Yuming Guo[a], Huijun Liang[c,*], Zhansheng Lu[d], Lin Yang[a,*], Hua Zhang[a] and Xiaoming Ma[a,*]

[a] Collaborative Innovation Center of Henan Province for Green Manufacturing of Fine Chemicals, Key Laboratory of Green Chemical Media and Reactions, Ministry of Education, School of Chemistry and Chemical Engineering, Henan Normal University, Xinxiang, Henan 453007, P. R. China

[b] Key Laboratory for Micro-Nano Energy Storage and Conversion Materials of Henan Province, College of Advanced Materials and Energy, Institute of Surface Micro and Nano Materials, Xuchang University, 88 Bayi Road, Xuchang 461000, P. R. China.

[c] School of Chemistry and Materials Engineering, Xinxiang University, Xinxiang, Henan 453003, P. R. China

[d] School of Physics, Henan Normal University, Xinxiang 453007, P. R. China

1. Supplementary experimental section

1.1. Materials

Oxalic acid dihydrate ($C_2H_2O_4 \cdot 2H_2O$, 99.5%), Tetrabutyl titanate (TBOT, 98.0%), Ethanol (C_2H_5OH, 99.7%), Palladium(II) chlorid ($PdCl_2$, 59.0%), Ferrous chloride tetrahydrate ($FeCl_2 \cdot 4H_2O$, 99.0%)were obtained from Sinopharm Chemical Reagent Co., Ltd. (Shanghai, China). Hydrochloric acid (HCl, 36-38%) and potassium thiocyanate (KSCN, 98.5%) were purchased from Luoyang Chemical Reagent Factory (Henan, China). and Suzhou Chemical Reagent Factory (Zhejiang, China), respectively. All the reagents were used without further purification.

1.2. Preparations of photocatalysts

1.2.1. Preparations of TiO_2-TELM

TiO_2-TELM samples were synthesized by a facile solvothermal reaction followed by annealing. First, $C_2H_2O_4 \cdot 2H_2O$ (10 g) was completely dissolved in absolute ethanol (57 mL) under vigorous magnetic stirring for 10 min. Second, TBOT (4 mL) was added into the above transparent solution and ultrasound-dispersed for 5 min. Then, HCl (12 M, 6 mL) was added under vigorous stirring for 1 min to obtain a light yellow transparent solution. After that, the solution was transferred to a 100 mL Teflon-lined autoclave and maintained temperature at 150 ºC for 15 h. After cooling down to room temperature, the white precipitates were collected by centrifugation at 5000 rpm for 10 min, followed by washed with absolute ethanol for three times, and dried in vacuum at 60 ºC to obtain the precursor of TiO_2-TELM sample. Subsequently, TiO_2-TELM was obtained by annealing the precursor at 400 ºC in air for 5 h.

Following the same procedures as that for the TiO_2-TELM of 15 h, the TiO_2-TELM at different time were synthesized, except for that the time of solvothermal reaction was adjusted to 5 and 15 min, 2, 5, 10, 20, and 25 h, respectively.

1.2.2. Preparations of Pd-TiO_2

Pd-TiO_2 composites were synthesized by the light-induced reduction method. First, 0.5 g as-prepared TiO_2-TELM powders were dispersed in 250 mL deionized water under magnetic stirring. Then, the suspension was transferred into a quartz reactor that was held at 10 ºC by a water-cooled jacket and irradiated by a 300 W Xenon lamp for 1 h. After that, 10 mL $PdCl_2$ aqueous solution (22.6 mM) was added and continuous irradiated for 15 min. Finally, the suspension was centrifuged, washed with deionized water and ethanol, and dried in vacuum at 60 ºC for 12 h. Pd-TiO_2 composites were obtained.

1.3. Characterizations

The purity and crystallinity of the as-prepared samples were characterized by X-ray diffraction (XRD, X'Pert^3 Powder XRD with Cu Kα radiation, λ = 0.154 nm, the accelerating voltage was set at 45 kV with a 40 mA flux, a step length of 0.1° and a preset time of 1 s/step). The morphologies and structure of the as-prepared samples were examined with transmission electron microscope (TEM, JEOL JEM-2100), high-resolution transmission electron microscopy (HRTEM, FEI Talos F200X), and field emission scanning electron microscopy (FESEM, Hitachi SU8010, an accelerating voltage of 200 kV). Diffuse reflection spectra (DRS) were obtained for the dry-pressed disk samples on a UV-vis spectrometer (Lambda950, PerkinElmer, America), and $BaSO_4$ was used as a reflectance standard. The steady-state and time-resolved transient photoluminescence (PL) measurements of samples were performed on an FLS980 fluorescence spectrometer (Edinburgh, U.K.) at room temperature, the excitation wavelength is 373 and 405 nm, respectively. The valence band XPS spectra were measured by X-ray photoelectron spectroscopy (XPS, Thermo Fisher EscaLab Xi^+, using Al Kα X-ray source with 10 mA at 15 kV). Electron paramagnetic resonance spectra (EPR) of radicals were recorded under Ar ambiance at room temperature on a Bruker EPR spectrometer (A300). Superoxide radicals ($•O_2^-$) and hydroxyl radicals (•OH) was detected by trapping with 100 mM of 5, 5-dimethyl-1-pyrroline N-oxide (DMPO) using methanol and water as solvent, respectively. The sample was detected under dark or under irradiation with a 300 W Xenon lamp (PLS-SXE300D, Beijing Perfectlight Technology Co., Ltd.). All EPR spectra were recorded under the same condition for 2 and 10 min: microwave frequency, 9.85 GHz; center field, 3510 G; sweep width, 100 G; modulation frequency, 100 kHz; and power, 19.31 mW. The transient-state surface photovoltage was investigated on a home-made capacitor-like spectroscope,[1] where a Quantel Nd:YAG nanosecond laser (Brilliant Eazy, BRILEZ/IR) was used as the excitation source (355 nm, 4 ns, spot area of 0.24 cm^2), coupled with a digital oscilloscope (Tektronix, TDS 3054C, 500 MHz) and pre-amplifier for recording.

1.4. Catalyst activity measurements

Photocatalytic water splitting experiments was conducted in a Pyrex top-irradiation vessel connected to a glass gas-closed circulation system (Labsolar-III, Beijing Perfectlight Technology Co., Ltd.). A 300 W Xenon lamp was used as the simulated solar irradiation (AM 1.5 G, 100 mW cm^{-2}), and the temperature of the reaction system was controlled at 25 °C by circulating cooling water. 25 mg of photocatalyst was dispersed in 50 mL deionized water (The electrical conductivity of deionized water is approximately 4.7 μS cm^{-1}.). Subsequently, the system was deoxygenated with

Ar for 30 min to remove the air before irradiation. The quantities of evolved gas were measured by an on-line gas chromatograph (GC-2014Plus, Shimadzu) with a TCD detector and Ar as carrier gas.

The apparent quantum efficiency was calculated using：A 300 W Xe lamp with an AM 1.5G filter was used as light source.

Apparent quantum efficiency (AQE):

$$AQEs(\%) = \frac{N_e}{N_p} \times 100\%$$

$$= \frac{10^9(v \times N_A \times K) \times (h \times c)}{(I \times A \times \lambda)} \times 100\%$$

where N_p is Number of incident photons, N_e is Number of electrons transferred by the reaction, I is the power density of the light source (W m^{-2}), A is the area of irradiation measured (m^2), λ is the wavelength absorbed by the photocatalyst (nm), v is the rate of hydrogen formation per second（mol s^{-1}）, N_A is Avogadro's number (6.02×10^{23} mol), K is Number of transferred electrons, h is Planck's constant (6.62×10^{-34} J s), and c is the light velocity (3×10^8 m s^{-1}).

During the photocatalytic pure water splitting, the content of H_2O_2 produced was measured by UV-vis spectrophotometer (TU-1900, Beijing). Because Fe^{2+} can be oxidized into Fe^{3+} by H_2O_2 in an acidic environment (pH=1~2), and Fe^{3+} can be combined by KSCN to form $[Fe(SCN)]^{2+}$, which has a maximum absorption peak at 475 nm.[2]

1.5. Photoelectrochemical and electrochemical measurements

The Mott-Schottky curves, photocurrent with ON/OFF cycles and electrochemical impedance spectra (EIS) were measured on an electrochemical workstation (CHI660E, Shanghai Chenhua, China) and carried out in a three-electrode system with a working electrode, Pt foil as the counter electrode, Ag/AgCl (saturated KCl) as reference electrode, respectively. 0.5 M Na_2SO_4 aqueous solution was used as the electrolyte solution. A 300 W Xenon lamp (Beijing Perfect Light Co., China) was utilized as the light source.

The working electrode was prepared as follows: 10 mg as-prepared TiO_2-TELM samples was ultrasonically dispersed in 0.5 mL absolute ethanol for 30 min, then, 0.2 mL as-obtained suspension was loaded onto an FTO glass electrode (1.2 cm×2.5 cm) drying at 60 ºC for 4 h. The catalyst on the FTO was about 1.33 mg cm^{-2}.

Mott-Schottky plots were obtained at a frequency of 1000 Hz. The potential ranged from 1.0 to -2.0 V (vs. Ag/AgCl). The photocurrent with ON/OFF cycles was measured under chopped light irradiation at 0.6 V (vs. Ag/AgCl) potential. Electrochemical impedance spectra (EIS) were collected in the frequency range from 0.01 to 1 MHz with a 5 mV sinusoidal AC voltage.

1.6. The semi-quantitative calculation of rutile (W_R) mass ratio

According to the reference intensity ratio (RIR) methods and the XRD peak intensity (I),[1] the mass ratio of rutile (W_R) can be semi-quantitative represented as:

$$W_R=I_R/(I_R+I_A*RIR_R/ RIR_A)$$

Where I_R and I_A refer to the intensities of the rutile (110) and anatase (101) diffraction peaks, the RIR_R and RIR_A is respectively 3.4 and 3.3 according to the JCPDS No. 21-1276 and JCPDS No. 21-1272.

1.7. The calculation of RHE

To remove the Nernstian pH-dependence of flat band potentials (E_{fb}), we further refer the E_{fb} values against the reversible hydrogen electrode (RHE):

$$E_{RHE} =E_{Ag/AgCl}+0.0592\ pH+E_{0,\ Ag/AgCl}$$

Where the pH value of the Na_2SO_4 electrolyte is 7.63, E_{RHE} is the converted potential versus RHE, $E_{0,Ag/AgCl}$ = 0.197 V at 25 **ºC**, and $E_{Ag/AgCl}$ is the experimentally measured potential against the $E_{0,Ag/AgCl}$ reference electrode.[2]

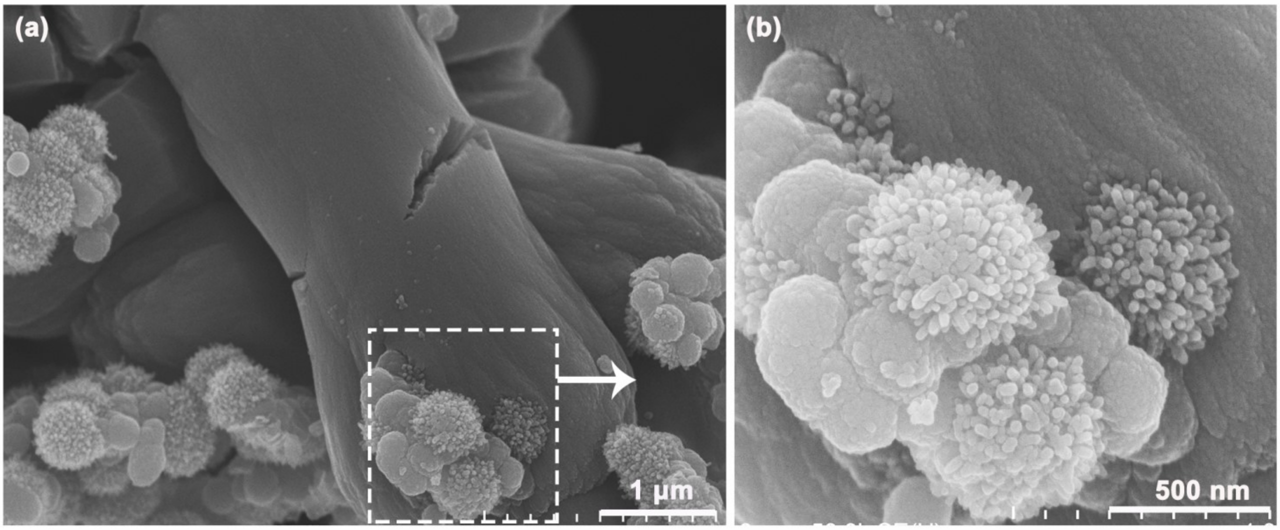

Fig. S1 Different magnification FESEM images of as-prepared TiO_2-TELM at 15 min, which was annealed at 400 ℃ in air for 5 h.

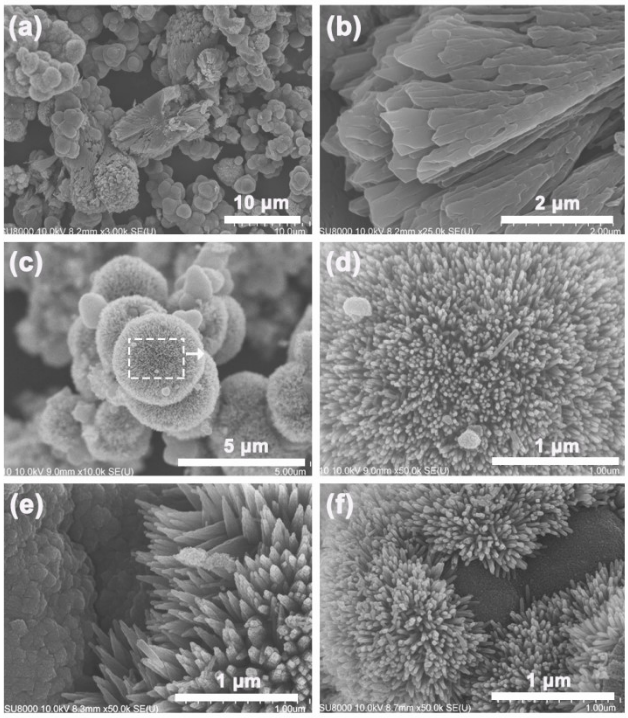

Fig. S2 Different magnification FESEM images of TiO_2-TELM precursors at the different reaction time, (a) and (b) 5 h, (c) and (d) 25 h, annealing before (e) and after (f) of TiO_2-TELM 15 h.

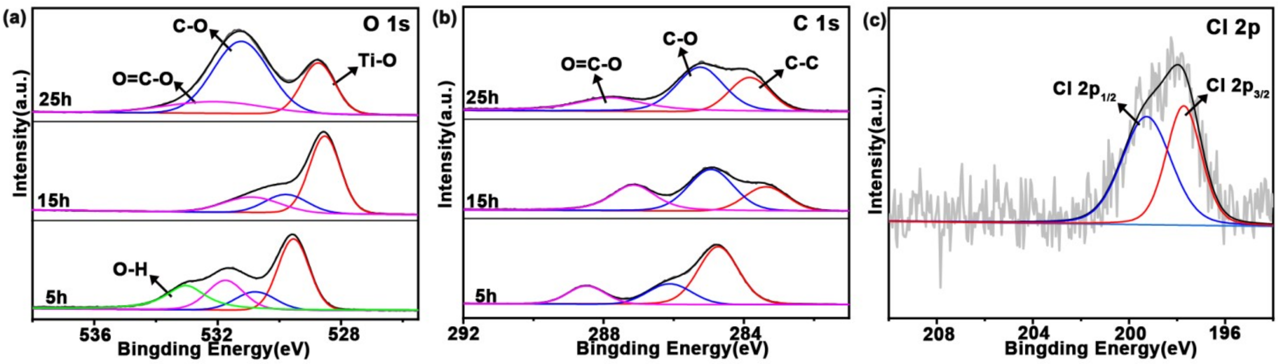

Fig. S3 High-resolution XPS spectra of (a) O 1s, (b) C 1s and (c) Cl 2p, respectively.

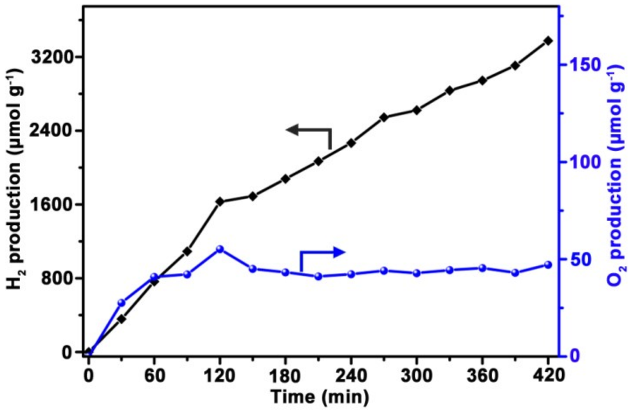

Fig. S4 Photocatalytic H_2 and O_2 evolution activities of as-prepared Pd-TiO_2 composites (15 h).

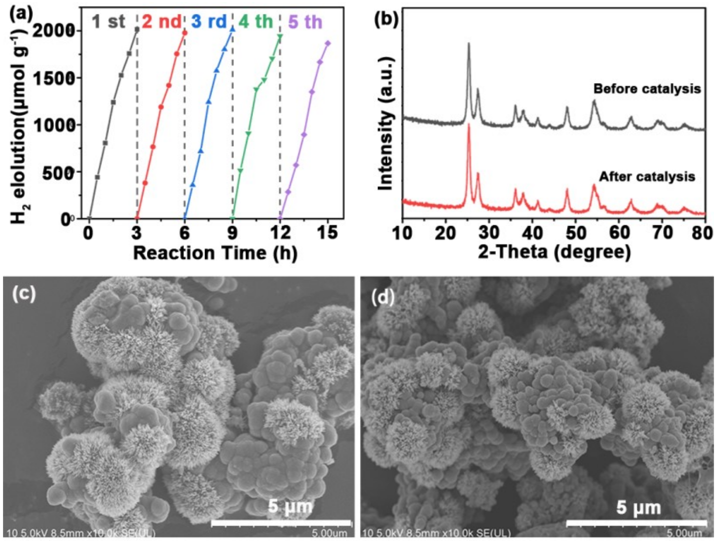

Fig. S5 (a) Photocatalytic stability of the Pd-TiO_2 composites (15 h) photocatalyst. (b) XRD patterns of Pd-TiO_2 (15 h) before and after catalysis. FESEM images of Pd-TiO_2 (15 h) before (c) and after catalysis (d).

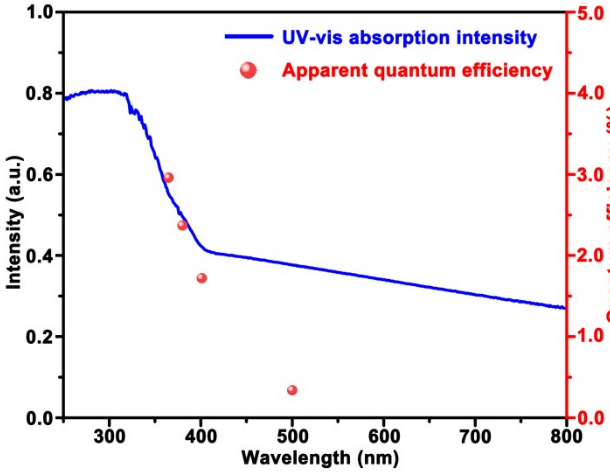

Fig. S6 Wavelength dependence of AQE of Pd-TiO_2 (15 h).

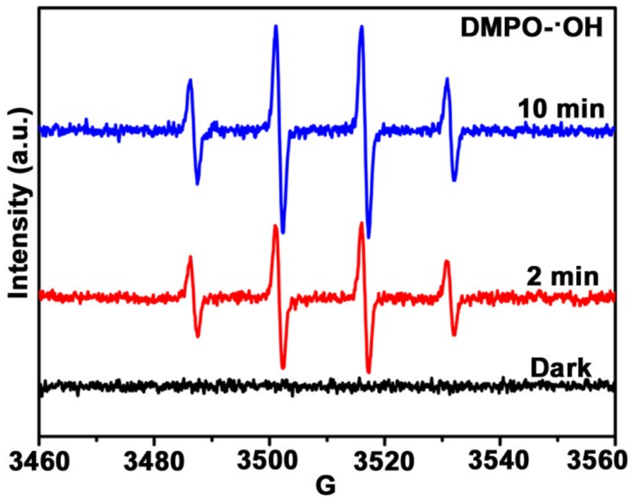

Fig. S7 Typical EPR spectra for photocatalytic splitting H_2O on Pd-TiO_2 in the presence of DMPO as an electron trapping agent. The signals were collected under light irradiation. Without light irradiation, no signal was detected. Conditions: DMPO, 100 mM; in Ar; irradiation time, 2 and 10 min; light Source: 300 W Xe lamp.

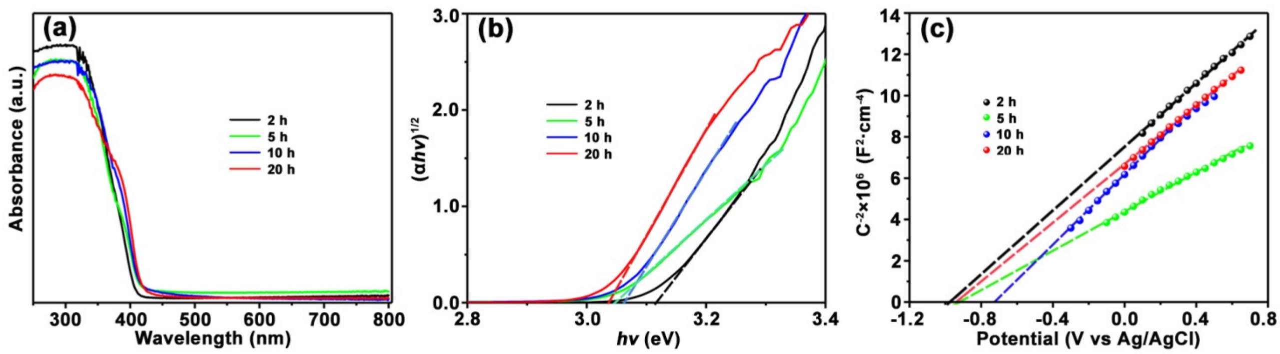

Fig. S8 (a) UV-vis DRS, (b) Tauc plots, and (c) Mott-Schottky plots for as-prepared TiO_2-TELM samples.

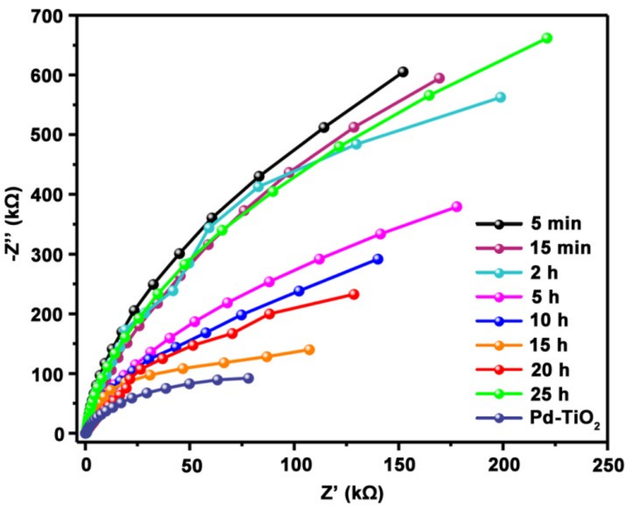

Fig. S9 Nyquist plots of electrochemical impedance spectra (EIS) for as-prepared TiO_2-TELM samples and Pd-TiO_2.

Table S1. Comparison of the photocatalytic H_2 evolution efficiency between previous reports and Pd-TiO_2 photocatalysts on the water splitting.

No.	**Catalysts**	**Cocatalyst**	Catal. /water (mg/mL)	**Light** source	**H_2 rate (μmol h^{-1} g^{-1})**	**O_2 or (H_2O_2) rate (μmol h^{-1} g^{-1})**	**Ref.**
1.	TiO_2(A)/TiO_2(R)	1% Pd	25/50	300 W Xe lamp	816/(2h)	O_2 and H_2O_2	This work
2.	TiO_2(A)/TiO_2(R)	Pt/CoP	20/100	300 W Xe lamp	614	297	3
3.	Rutile TiO_2 (111)/(101)	1% Pt	50/100	100 W Hg lamp	566/(2h)	--	4
4.	TiO_2(A)/TiO_2(B)/TiO_2(R)	N-doped	5/50	Sun light	192	--	5
5.	TiO_2(B) big/small	0.5 wt % Pt	50/100	300 W Xe lamp	149	--	6
6.	Pt/TiO_2	--	--	300 W Xe lamp	62.9	31.5	7
7.	TiO_2(R)	0.2wt% Pt	50/150	300 W Xe lamp	33.8	16.6	8
8.	CdS/Pt-N-TiO_2	0.5%-Pt	50/275	125 W Hg lamp	639.2	319	9
9.	$Ti_3C_2T_x$@TiO_2	Black P	10/100	300 W Xe lamp	564.8	400(H_2O_2)	10
10.	Ti_3C_2–TiO_2	Pt	20/100	300 W Xe lamp	526	315	11
11.	Ti_3C_2(TiO_2)@CdS/MoS_2	--	30/100	300 W Xe lamp	344.74	--	12
12.	0D/2D TiO_2 /g-C_3N_4	3% Pt	10/25	300 W Xe lamp	329.5	159.6	13
13.	Fe_2O_3–TiO_2	--	1/20	150 W Xe lamp	323	--	14
14.	GaP-TiO_2-SiO_2	0.3wt% Pt	500/100	300 W Xe lamp	80.1	41.2	15
15.	Co_3O_4/TiO_2	--	50/100	300 W Xe lamp	41.8	24.2	16
16.	g-$C_3N_{3.5}$($O_{0.5}H_{0.5}$)	2 wt % Pt	30/100	300 W Xe-lamp	947.7	67.2	17

No.	**Catalysts**	**Cocatalyst**	Catal. /water (mg/mL)	**Light** source	**H_2 rate (μmol h^{-1} g^{-1})**	**O_2 or (H_2O_2) rate (μmol h^{-1} g^{-1})**	**Ref.**
17.	CdS/g-C_3N_4	Pt and MnO_x	10/100	300 W Xe lamp	924.4	460	18
18.	10% Ni_2P/CdS	Artificial gill	100/150	300 W Xe lamp	837.9	450	19
19.	$BiFeO_3$/CdS	--	200/100	125 W Hg lamps	600.2	300	20
20.	C-dot/g-C_3N_4	--	10/150	300 W Xe lamp	568	301	21
21.	C_{co}-C_3N_4	--	30/80	300 W Xe lamp	530	255	22
22.	$SrTiO_3$(Al)/CoO_x	Ni SA-NG	50/100	280 W Xe lamp	498	230	23
23.	Fe/MgO-rGO	--	20/30	500 W Hg-Xe lamp	450	--	24
24.	$MnPSe_3$	--	20/100	AM 1.5G	325	--	25
25.	$BiVO_4$/Au/CdS	--	30/100	100 W Xe lamp	281	138	26
26.	P-doped $Mn_xCd_{1-x}S/Ni_2P$	--	30/40	300 W Xe lamp	251	--	27
27.	$Cd_{0.5}Zn_{0.5}S$	--	10/100	300 W Xe lamp	248	--	28
28.	5%CoP/CdS-P	--	5/20	white LED light	231	H_2O_2	29
29.	Co-doped g-C_3N_4	--	10/25	white LED light	182	165(H_2O_2)	30
30.	CZS-C-P5	--	20/100	300 W Xe lamp	137.2	123.8	31
31.	Fe_2O_3@MnO_2/ C_3N_4	--	30/80	300 W Xe lamp	124	--	32
32.	MoO_3/N-MoS_2	--	50/70	400 W Xe lamp	118	--	33

A — anatase, B — brookite, R — rulite

References

1. L. Li, X. Yang, Y. Lei, H. Yu, Z. Yang, Z. Zheng and D. Wang, Ultrathin Fe-NiO nanosheets as catalytic charge reservoirs for a planar Mo-doped $BiVO_4$ photoanode, *Chem. Sci.*, 2018, **9**, 8860-8870.
2. H.-F. Ye, R. Shi, X. Yang, W.-F. Fu and Y. Chen, P-doped $Zn_xCd_{1−x}S$ solid solutions as photocatalysts for hydrogen evolution from water splitting coupled with photocatalytic oxidation of 5-hydroxymethylfurfural, *Appl. Catal. B: Environ.*, 2018, **233**, 70-79.
3. L. Ding, S. Yang, Z. Liang, X. Qian, X. Chen, H. Cui and J. Tian, TiO_2 nanobelts with anatase/rutile heterophase junctions for highly efficient photocatalytic overall water splitting, *J. Coll. Interf. Sci.*, 2020, **567**, 181-189.
4. C. Gao, T. Wei, Y. Zhang, X. Song, Y. Huan, H. Liu, M. Zhao, J. Yu and X. Chen, A photoresponsive rutile TiO_2 heterojunction with enhanced electron-hole separation for high-performance hydrogen evolution, *Adv. Mater.*, 2019, **31**, e1806596.
5. P. A. K. Reddy, P. V. L. Reddy, K.-H. Kim, M. K. Kumar, C. Manvitha and J.-J. Shim, Novel approach for the synthesis of nitrogen-doped titania with variable phase composition and enhanced production of hydrogen under solar irradiation, *J. Ind. Eng. Chem.*, 2017, **53**, 253-260.
6. Y. Bai, Y. Zhou, J. Zhang, X. Chen, Y. Zhang, J. Liu, J. Wang, F. Wang, C. Chen, C. Li, R. Li and C. Li, Homophase junction for promoting spatial charge separation in photocatalytic water splitting, *ACS Catal.*, 2019, **9**, 3242-3252.
7. Y. Zhang, H. Hu, X. Huang and Y. Bi, Photo-controlled bond changes on Pt/TiO_2 for promoting overall water splitting and restraining hydrogen–oxygen recombination, *J. Mater. Chem. A*, 2019, **7**, 5938-5942.
8. R. Li, Y. Weng, X. Zhou, X. Wang, Y. Mi, R. Chong, H. Han and C. Li, Achieving overall water

splitting using titanium dioxide-based photocatalysts of different phases, *Energy Environ. Sci.*, 2015, **8**, 2377-2382.

9. M. Solakidou, A. Giannakas, Y. Georgiou, N. Boukos, M. Louloudi and Y. Deligiannakis, Efficient photocatalytic water-splitting performance by ternary CdS/Pt-N-TiO_2 and CdS/Pt-N,F-TiO_2: Interplay between CdS photo corrosion and TiO_2-dopping, *Appl. Catal. B: Environ.*, 2019, **254**, 194-205.
10. Z. Ai, K. Zhang, L. Xu, M. Huang, D. Shi, Y. Shao, J. Shen, Y. Wu and X. Hao, In situ configuration of dual S-scheme BP/($Ti_3C_2T_x$@TiO_2) heterojunction for broadband spectrum solar-driven photocatalytic H_2 evolution in pure water, *J. Colloid Interface Sci.*, 2022, **610**, 13-23.
11. Y. Li, X. Deng, J. Tian, Z. Liang and H. Cui, Ti_3C_2 MXene-derived Ti_3C_2/TiO_2 nanoflowers for noble-metal-free photocatalytic overall water splitting, *Appl. Mater.Today*, 2018, **13**, 217-227.
12. Z. Ai, Y. Shao, B. Chang, B. Huang, Y. Wu and X. Hao, Effective orientation control of photogenerated carrier separation via rational design of a Ti_3C_2(TiO_2)@CdS/MoS_2 photocatalytic system, *Appl. Catal. B: Environ.*, 2019, **242**, 202-208.
13. Y. Jiang, Z. Sun, Q. Chen, C. Cao, Y. Zhao, W. Yang, L. Zeng and L. Huang, Fabrication of 0D/2D TiO_2 Nanodots/g-C_3N_4 S-scheme heterojunction photocatalyst for efficient photocatalytic overall water splitting, *Appl. Sur. Sci.*, 2022, **571**, 151287.
14. T. C. Bhagya, A. Krishnan, A. R. S, A. S. M, B. R. Sreelekshmy, P. Jineesh and S. M. A. Shibli, Exploration and evaluation of proton source-assisted photocatalyst for hydrogen generation, *Photochem. Photobiol. Sci.*, 2019, **18**, 1716-1726.
15. H. V. Dang, Y. H. Wang and J. C. S. Wu, Z-scheme photocatalyst Pt/GaP-TiO_2-SiO_2:Rh for the separated H_2 evolution from photocatalytic seawater splitting, *Appl. Catal. B: Environ.*, 2021,

296, 120339.

16. J. Liu, J. Ke, Y. Li, B. Liu, L. Wang, H. Xiao and S. Wang, Co_3O_4 quantum dots/TiO_2 nanobelt hybrids for highly efficient photocatalytic overall water splitting, *Appl. Catal. B: Environ.*, 2018, **236**, 396-403.
17. W. Che, H. Su, X. Zhao, Y. Li, H. Zhang, W. Zhou, M. Liu, W. Cheng, F. Hu and Q. Liu, An on-demand solar hydrogen-evolution system for unassisted high-efficiency pure-water splitting, *J. Mater. Chem. A*, 2019, **7**, 17315-17323.
18. X. Zhou, Y. Fang, X. Cai, S. Zhang, S. Yang, H. Wang, X. Zhong and Y. Fang, In situ photodeposited construction of Pt–CdS/g-C_3N_4–MnO_x composite photocatalyst for efficient visible-light-driven overall water splitting, *ACS Appl. Mater. Interfaces*, 2020, **12**, 20579-20588.
19. W. Zhen, X. Ning, B. Yang, Y. Wu, Z. Li and G. Lu, The enhancement of CdS photocatalytic activity for water splitting via anti-photocorrosion by coating Ni_2P shell and removing nascent formed oxygen with artificial gill, *Appl. Catal. B: Environ.*, 2018, **221**, 243-257.
20. A. Kolivand and S. Sharifnia, Enhanced photocatalytic hydrogen evolution from water splitting by Z‐scheme CdS/$BiFeO_3$ heterojunction without using sacrificial agent, *Int. J. Energy Res.*, 2020, **45**, 2739-2752.
21. J. Liu, Y. Liu, N. Liu, Y. Han, X. Zhang, H. Huang, Y. Lifshitz, S. T. Lee, J. Zhong and Z. Kang, Water splitting. Metal-free efficient photocatalyst for stable visible water splitting via a two-electron pathway, *Science*, 2015, **347**, 970-974.
22. X. Fang, R. Gao, Y. Yang and D. Yan, A cocrystal precursor strategy for carbon-rich graphitic carbon nitride toward high-efficiency photocatalytic overall water splitting, *IScience*, 2019, **16**, 22-30.

23. Y. Liu, X. Xu, S. Zheng, S. Lv, H. Li, Z. Si, X. Wu, R. Ran, D. Weng and F. Kang, Ni single atoms anchored on nitrogen-doped graphene as H_2-Evolution cocatalyst of $SrTiO_3$(Al)/CoO for photocatalytic overall water splitting, *Carbon*, 2021, **183**, 763-773.
24. F. Sharmin, D. Chandra Roy and M. A. Basith, Photocatalytic water splitting ability of Fe/MgO-rGO nanocomposites towards hydrogen evolution, *Int. J. Hydrogen Energy*, 2021, **46**, 38232-38246.
25. T. A. Shifa, F. Wang, Z. Cheng, P. He, Y. Liu, C. Jiang, Z. Wang and J. He, High crystal quality 2D manganese phosphorus trichalcogenide nanosheets and their photocatalytic activity, *Adv. Funct. Mater.*, 2018, **28**, 1800548.
26. X. Xu, Z. Wang, W. Qiao, F. Luo, J. Hu, D. Wang and Y. Zhou, Refined Z-scheme charge transfer in facet-selective $BiVO_4$/Au/CdS heterostructure for solar overall water splitting, *Int. J. Hydrogen Energy*, 2021, **46**, 8531-8538.
27. J. Yan and L. Shi, The preparation of 0D/2D P‐doped $MnxCd_{1-x}S/Ni_2P$ photocatalyst and its photocatalytic activity of pure water splitting for H_2, *Int. J. Energy Res.*, 2022, **46**, 8218-8228.
28. W. Xue, X. Bai, J. Tian, X. Ma, X. Hu, J. Fan and E. Liu, Enhanced photocatalytic H_2 evolution on ultrathin $Cd_{0.5}Zn_{0.5}S$ nanosheets without a hole scavenger: Combined analysis of surface reaction kinetics and energy-level alignment, *Chem. Eng. J.*, 2022, **428**, 132608.
29. R. Shi, H.-F. Ye, F. Liang, Z. Wang, K. Li, Y. Weng, Z. Lin, W.-F. Fu, C.-M. Che and Y. Chen, Interstitial P-doped CdS with long-lived photogenerated electrons for photocatalytic water splitting without sacrificial agents, *Adv. Mater.*, 2018, **30**, 1705941.
30. Y. Dou, C. Zhu, M. Zhu, Y. Fu, H. Wang, C. Shi, H. Huang, Y. Liu and Z. Kang, Highly mesoporous carbon nitride photocatalysts for efficient and stable overall water splitting, *Appl.

Surf. Sci., 2020, **509**, 144706.

31. F. Liu, F. Xue, Y. Si, G. Chen, X. Guan, K. Lu and M. Liu, Functionalized $Cd_{0.5}Zn_{0.5}S$ chalcogenide nanotwins enabling Z-scheme photocatalytic water splitting, *ACS Appl. Nano Mater.*, 2021, **4**, 759-768.

32. N. Wang, L. Wu, J. Li, J. Mo, Q. Peng and X. Li, Construction of hierarchical Fe_2O_3@MnO_2 core/shell nanocube supported C_3N_4 for dual Z-scheme photocatalytic water splitting, *Sol. Energy Mater. Sol. Cells*, 2020, **215**, 110624.

33. N. R. Khalid, M. Rizwan Kamal, M. B. Tahir, M. Rafique, N. A. Niaz, Y. Ali, M. Alzaid, H. Alrobei and S. Muhammad, Fabrication of direct Z-scheme MoO_3/N–MoS_2 photocatalyst for synergistically enhanced H_2 production, *Int. J. Hydrogen Energy*, 2021, **46**, 39822-39829.